ORIGINAL PAPER

Coseismic landslide hazard assessment for the future scenario earthquakes in the Kumaun Himalaya, India

Sandeep Kumar[1] · Vikram Gupta[1] · Parveen Kumar[1] · Y. P. Sundriyal[2]

Abstract

The coseismic landslide is one of the important hazard phenomena in the hilly and seismically active mountainous region. It is, therefore, essential to map the areas susceptible to coseismic landslides, especially for the seismically active region.

In the present work, the probabilistic assessment of coseismic landslides has been carried out for Goriganga valley located in the Kumaun Himalaya, India, which lies in the highest seismically active zone of the seismic zoning map of India. Several studies suggest that this region is prone to a great future earthquake of Mw ≥8.0.

In this context, mapping of the coseismic landslide has been made for the future scenario earthquakes of 7.0, 8.0, and 8.6 Mw using modified Newmark's analysis. The modified Newmark's analysis provides the permanent displacement of the potential landslide, by integrating (1) joint strength of rock mass, (2) critical acceleration of the slope, and (3) peak ground acceleration of the region. Newmark permanent displacement has been estimated, which provides the distribution of predicted slope failure in the area.

It has been observed that 41% of the area exhibits >40 cm Newmark's permanent displacement corresponding to Mw 8.6 earthquake and thus susceptible to failure, followed by 8.0 and 7.0 Mw earthquake with 36 and 14% of the area susceptible to the coseismic landslide, respectively. Further, the maximum permanent displacements for the simulated earthquakes of Mw 7.0, 8.0, and 8.6 are 76, 279, and 502 cm, respectively.

Keywords Coseismic landslide · Himalaya · Dynamic slope stability · Newmark analysis · Seismic

Introduction

Landslides are caused by numerous geological, geomorphological, and anthropogenic factors but are generally triggered by rainfall and earthquake vibrations (Cruden 1991; Haque et al. 2019). In the tectonically active mountainous terrains, earthquake is one of the major triggering factors for the occurrence of landslides (Keefer 1984; Youd 1985; Jibson et al. 2000; Xu et al. 2013), and many a time, it has been noticed that the destruction caused due to the earthquake-induced landslides is much greater than the destruction caused by direct ground shaking of an earthquake (Keefer 1984; Jibson et al. 2000; Dunning et al. 2007). These landslides cause immense loss of lives and damage to lifeline infrastructures such as water and gas pipelines, schools, and hospitals, roads, and drainage; hence, these kinds of landslides are one of the most important geohazards in the seismically active hilly region. For examples, the 1999 Chi-Chi, Taiwan earthquake ($M_w = 7.6$) triggered >9272 landslides, which cause several causalities and damage to the infrastructure (Lin and Tung, 2004), and the 2008 Wenchuan, China, earthquake ($M_w = 7.9$) triggered >15,000 landslides, killing ~20,000 people, and this accounts for one-fourth of the total deaths due to the earthquake (Yin et al. 2009).

Earthquake-induced landslides are very common in the Himalaya and its surrounding regions. There are many recent examples of earthquake-induced landslides from the Himalayan terrain, such as the 2005 Kashmir earthquake ($M_w = 7.6$) triggered 2424 landslides (Owen et al. 2008), 2011 Sikkim earthquake, India ($M_w = 6.9$) triggered 1196 landslides (Martha et al. 2015), the 2013 Lushan, earthquake, China ($M_w = 6.6$) triggered 4540 landslides (Ma and Xu 2019), the 2014 Ludian earthquake, China ($M_w = 6.1$) triggered 1826 landslides (Zhou et al. 2016; Chen et al. 2019),

✉ Vikram Gupta
   vgupta@wihg.res.in

1   Wadia Institute of Himalayan Geology, Dehardun, Uttarakhand 248
    001, India

2   HNB Garhwal University, Srinagar, Uttarakhand, India

and the 2015 Gorkha earthquake, Nepal (M_w = 7.8) triggered >2000 landslides (Roback et al. 2018). Most of these land-slides are classified as rockfalls, debris falls, rockslides, and debris slides (Keefer 1984; Owen et al. 2008).

There are many static and dynamic methods for the evaluation of landslides, like geomorphological landslide hazard mapping (Van Westen et al., 2000), analysis of landslide inventories (Guzzetti et al. 1994), index-based methods (Nilsen and Brabb 1977), statistically based modeling (Neuland 1976; Yin and Yan 1988), and physical-based modeling (Okimura and Kawatani 1987); however, earthquake-induced landslides are generally evaluated by physical-based models incorporating seismo-logical parameters, and the most commonly used seismic parameter is the peak ground acceleration (Wilson and Keefer 1983; Jibson et al. 2000; Jibson 2011; Zang et al. 2020). Newmark (1965) proposed a method, which considers that the landslide will occur when the seismic acceleration exceeds the critical acceleration, and the per-manent displacement of slope can be calculated using the acceleration time-history of the earthquake. The calculat-ed permanent displacement can be used to estimate the slope instability during an earthquake (Wu and Chen 1979; Wilson and Keefer 1983; Jibson et al. 2000; Wu and Lin 2008; Wu and Chen 2009; Wu and Tsai 2011; Shinoda and Miyata 2017; Hung et al. 2018; Romeo 2000; Yigit 2020; Zang et al. 2020; Yang et al. 2021). Gallen et al. (2017) have used Newmark's analysis for the estimation of permanent displacement of slopes in Nepal affected by the 2015 Gorkha earthquake, and Chen et al. (2018) have estimated the threshold value of ground ac-celeration for coseismic landslides in the Ludian, China region affected by the 2014 Ludian earthquake, China.

Various studies have been done on the coseismic landslides after the occurrence of an earthquake but the present study deals with the probabilistic assessment of coseismic landslides in the view of future scenarios. This study has been done using three simulated earthquakes of magnitude (M_w) 7.0, 8.0, and 8.6 in the Goriganga river valley, located in the Kumaon re-gion of northwest Himalaya, India. The area forms a part of the central seismic gap as it lies between the rupture zone of two great earthquakes, namely 1905 Kangra and 1934 Bihar Nepal earthquake, and is seismically an active part of the Himalayan arc (Khattri and Tyagi 1983).

Study area

The area for the present study is located between latitudes 29°44′58″N and 30°35′13″N and longitudes 80°02′25″E and 80°22′25″E. It is located on either side of the Goriganga River, a major tributary of the Kali River, and runs for a stretch of ~114 km between 10 km upstream of village Milam and

Jauljibi. It covers an area of ~2239 km^2 and is located in the Kumaun region in the state of Uttarakhand, India (Fig. 1).

Geologically, the area cuts across the Tethyan Sedimentary Sequence (TSS), the Higher Himalaya gneisses, and the Lesser Himalayan meta-sedimentaries (Fig. 1). These geolog-ical sections are separated from one another by the South Tibetan Detachment (STD) and the Vaikrita Thrust (VT) (Valdiya, 2001). The rocks constituting the TSS are mainly phyllite and are overlain over the gneisses belonging to the Higher Himalaya along the Vaikrita Thrust, which in turn is overlain over the Lesser Himalayan metasedimentaries, mainly constituting slate, limestone, dolomite, quartzite, gneisses, and schistose gneiss along the Munsiyari Thrust. The higher Himalayan gneisses are categorized into the Vaikrita Group of rocks (Valdiya 1980), whereas the Lesser Himalayan metasedimentaries are grouped under Munsiyari Formation, Beringag Formation, Manthali Formation, Gangolihat Formation, Rautgara Formation, and Chiplakot Crystalline. The Lesser Himalaya also con-stitutes gneissic rocks, which occur as Nappe termed as Chiplakot Crystallines or Chiplakot Nappe that is bounded by the North Chiplakot Thrust (NCT) in the North and South Chiplakot Thrust (SCT) in the South (Valdiya 1980). The geological setting of the area has been discussed in detail by Valdiya (1980), Valdiya (2001), Luirei et al. (2006). Two local faults, Baram Fault trending NNW-SSE and Rauntis Fault trending NW-SE traverses through the southern part of the study area (Luirei et al. 2006).

Geomorphologically, the area is rugged, having a relief of ~6833 m, with elevation varying between 556 and 7389 m. The slopes, in general, are steep to very steep varying between 40 and 70°. The northern part of the area between the Bodyar village and the Milam village dominantly exhibits glacial landforms, whereas fluvial topography dominates in the downstream region. Various geomorphic features like triangular facets, wa-terfalls, hot water springs, and terraces are observed in the area of study. The climate of the region is humid, with an average annual rainfall of ~2000 mm. The area facing the maximum temperature of 18.4°C and a min-imum of −2°C (Raj 2011; Yadav et al. 2014).

Seismically, the area falls in seismic zone V, the highest seismic activity zone on the seismic zoning map of India (BIS Code 1893 2002). This zone indicates the possibility of earthquakes of seismic intensity IX. The seismic intensity quantifies on the basis of modified Mercalli intensity scale (MMI) having a scale level from I to XII, which is scaled on the basis of human observation of shaking and damage during an earthquake. The shaking and damage due to the earth-quake increase as the scale level increases from I to XII (Wald et al. 1999). In addition, this region lies in the central seismic gap (CSG) of major earthquakes, and thus there is also a possibility of higher seismic activity (Khattri and
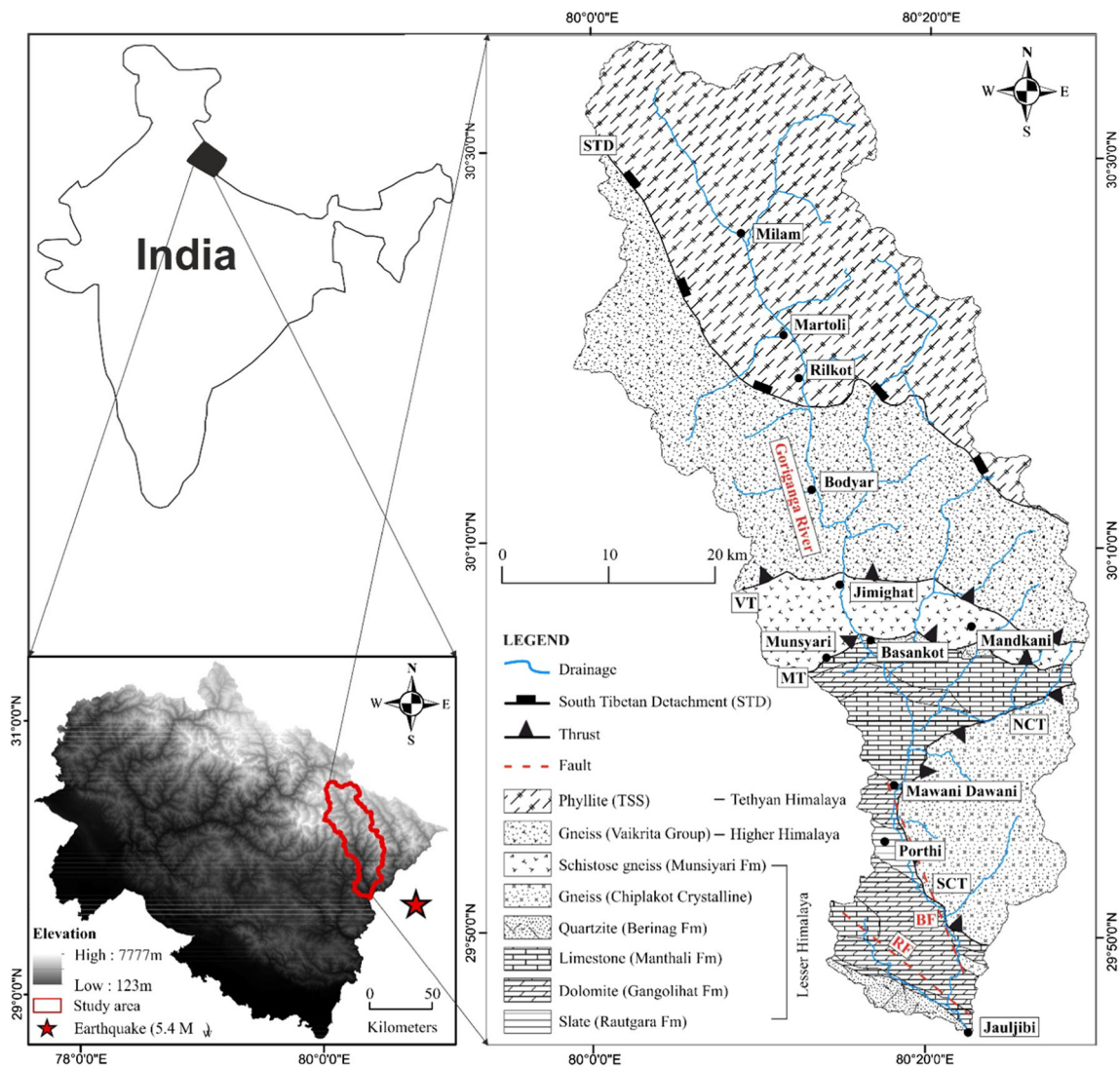
Fig. 1 The geological setup of the study region and epicenter of the earthquake. STD, South Tibetan Detachment; VT, Vaikrita Thrust; MT, Munsiyari Thrust; NCT, North Chiplakot Thrust; SCT, South Chiplakot Thrust; BF, Baram Fault; RF, Rauntis Fault

Tyagi 1983; Joshi et al. 2012; Kumar et al. 2015; Monika et al. 2020).

Methodology

In the present study, Newmark's analysis proposed by Newmark (1965) and later modified by Zang et al. (2020) for the joint strength of the rock mass has been adopted for the co-seismic landslide hazard assessment. Here, permanent displacement of rock mass along with critical acceleration of an inclined plane is introduced on the basis of a sliding-block model of Newmark analysis (Fig. 2). Figure 2a indicates the theoretical model of sliding-block on an inclined plane and Fig. 2b represents the unloading joints on a natural slope. The methodology used for the present study includes the calculation of (i) static factor of safety, (ii) critical acceleration,

(iii) peak ground acceleration, and (iv) Newmark's permanent displacement and the flowchart of the methodology is depicted in Fig. 3. Figure 3 illustrates that number of input parameters, i.e., geotechnical parameters, topographic parameter, and peak ground acceleration (PGA) are required to attain the Newmark's permanent displacement. In the first step, various geotechnical parameters (Unit weight: γ, Basic internal friction angle: Φ_b, Joint roughness coefficient: JRC_n, Joint wall compressive strength: JCS_n) and topographical parameter (Slope angle) are used to compute the static factor of safety. In the second step, the obtained static factor of safety and slope angle are further used to calculate the critical acceleration (a_c). Finally, the peak ground acceleration (PGA) and critical acceleration are utilized to estimate the final output in the form the Newmark's permanent displacement. The following procedure is adopted for the calculation of various parameters.

Fig. 2 (**a**) Theoretical sliding
block model for the Newmark
analysis, (**b**) The diagram
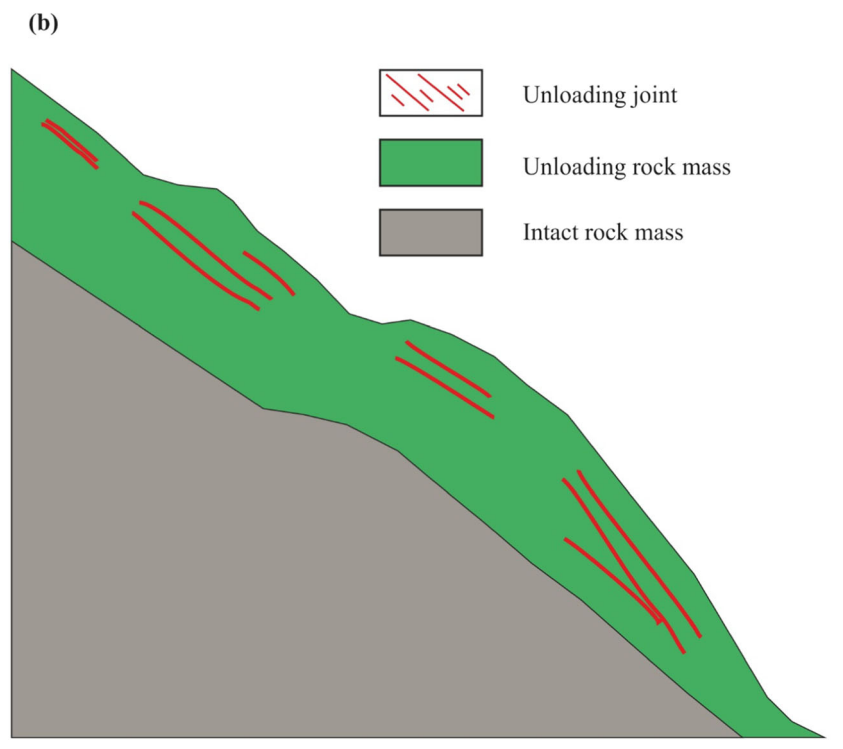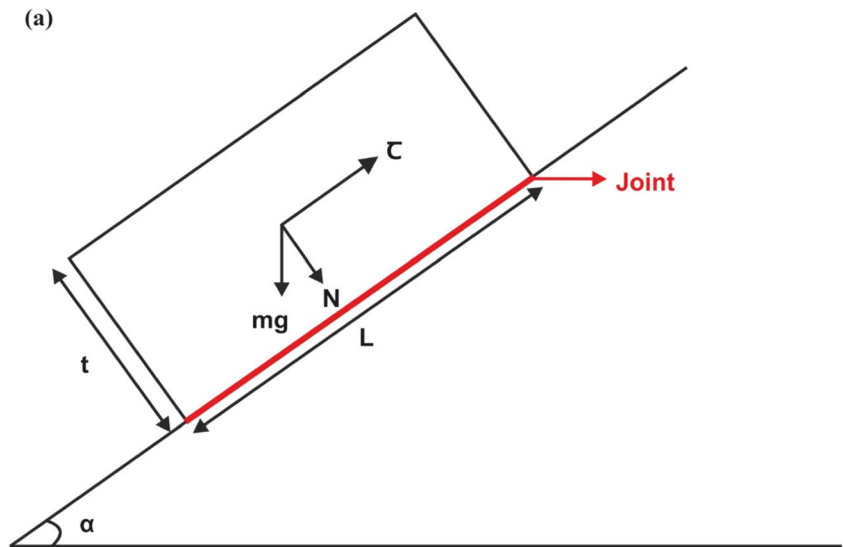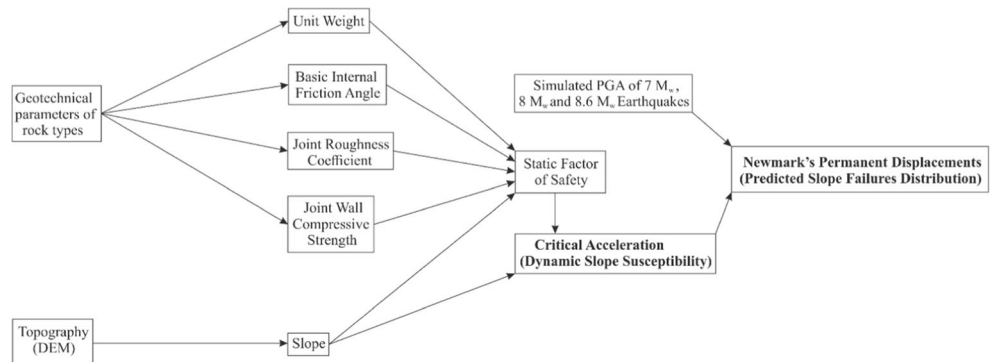showing shallow unloading joints
in the slope

Fig. 3 The flow-diagram of the
methodology for the Newmark
analysis adopted for the present
work

Geotechnical parameters

The geotechnical parameters of the rock mass (Joint roughness coefficient: JRC_n, Joint wall compressive strength: JCS_n, Unit weight: γ, Basic internal friction angle: Φ_b,) are estimated for the computation of static factor of safety. The JRC_n and JCS_n parameters are computed from the field investigation. The γ and Φ_b parameters are considered on the basis of the published work as reported in Table 1. The various input geotechnical parameters used for the calculation of the static factor of safety are given in Table 1.

Topographical parameter

The slope angle is one of the important input parameters needed to compute the static factor of safety and critical acceleration of slope. The slope angle is calculated from a high-resolution (12.5 × 12.5 m) digital elevation model (DEM) in the ArcGIS platform. The DEM data generated in August 2015 by Alaska Satellite Facility (ASF) is implemented for the same.

Static factor of safety

The obtained geotechnical and topographical parameters are implemented to compute the static factor of safety. The static factor of safety determines the stability of slopes without any external forces. It is expressed by the equation:-

$$F_s = \frac{Resisting\ Force}{Driving\ Force}$$

Barton (1973) modified the static factor of safety under the condition of unloading joints on the slopes, which is expressed as follow:

$$F_s = \frac{tan\left[JRC_n\left(\dfrac{JCS_n}{\gamma t cos\ \alpha}\right) + \Phi_b\right]}{tan\ \alpha} \tag{1}$$

Where JRC_n is the joint roughness coefficient, JCS_n is the joint surface compressive strength, γ is the unit weight of the rock block, t is the thickness of the failure rock block, which is considered as 3 m (Keefer 1984; Qi et al. 2012), Φ_b is the basic friction angle, α is the angle of the slope.

Critical acceleration

Subsequently, the computed static factor of safety and slope angle are used to assess the critical acceleration using the following formula (Newmark 1965):

$$a_c = (F_s - 1)g sin\ \alpha \tag{2}$$

Where, a_c is the critical acceleration in terms of g, F_s is the static factor of safety, α is the angle of slope along which the potential landslide block slides.

Peak ground acceleration

The peak ground acceleration (PGA) is computed for the study region. The PGA values are simulated at various grid points (0.1° × 0.1°) in the study region and these values are further used to prepare the PGA distribution map.

Newmark's permanent displacement

Finally, the Newmark's permanent displacement is calculated by utilizing the empirical regression model of critical acceleration, the peak ground acceleration, and the moment magnitude (M_w) using the following equation (Rathje and Saygili 2009):

Table 1 The parameters of the shear strength assigned to rock types for the present work

Rock types	γ (kN/m3)	Source	Φ (Deg.)	References	JCSn (MPa)	JRCn	Source
Phyllite	28.3	Rock Mechanics Database	28°	Duncan (1969)	68.6	3.3	Calculated from the field investigation
Gneiss	26.5		29°	Coulson (1972)	105.4	5.1	
Schistose gneiss	26.8		26°	Coulson (1972)	104.9	4.4	
Quartzite	26.9	Provided by Colorado School of Mines	44°	Duncan and Sheerman-Chase, 1965-1966)	105.9	6.2	
Limestone	21.5		31°	Duncan (1969)	57.7	5.7	
Dolomite	25.9		32°	Coulson (1972)	104.4	3.6	
Slate	26.5		25°	Barton (1971)	78.6	1.5	

$$ln\, D = 4.89 - 4.85 \left(\frac{\alpha_c}{PGA}\right) - 19.64 \left(\frac{\alpha_c}{PGA}\right)^2$$
$$+ 42.49 \left(\frac{\alpha_c}{PGA}\right)^3 - 29.06 \left(\frac{\alpha_c}{PGA}\right)^4$$
$$+ 0.72 ln\, (PGA) + 0.89\, (M_w - 6) \qquad (3)$$

Where D is the predicted permanent Newmark's displacement in centimeters, α_c is critical acceleration in g, PGA is peak ground acceleration in g, M_w is the moment magnitude of an earthquake. For the present study, PGA for the three scenarios earthquakes of M_w 7.0, 8.0, and 8.6 are considered for the estimation of Newmark's permanent displacement.

Results

The probabilistic coseismic landslide hazard has been assessed using parameters like static factor of safety, critical acceleration, peak ground acceleration, and Newmark's permanent displacement. These are briefly described hereunder.

Static factor of safety

The static factor of safety is the mathematical function of the rock strength and the slope angle of the surface. The slope map (Fig. 4) is prepared from a high-resolution DEM that enhances the accuracy of hazard assessment and preserves the insidious topographic features, in which many slope failures can occur. For the preparation of the slope map, comparison of the elevation of neighbor cells has been made to calculate the steepest downhill slope (Horn 1981). The hills that have an angle of slope steeper than 60° are unstable even at high strengths. The Newmark's analysis is not suitable for these steep slopes (>60°) and it provides very small values of the static factor of safety in these areas (Jibson et al., 2000). To overcome this problem, Zang et al. (2020) assigned an angle of slope (α) i.e. $\alpha = (45 + \Phi_b/2)$ to a steeper slope greater than 60°. Figure 4 depicts the distribution of inclination of the sloped surfaces in the area and it describes that very small regions experience steep slopes (>60°). As the DEM used in this work has a resolution of 12.5 × 12.5 m, so the digital geological map has also been rasterized at 12.5 m grid cells for assigning the rock strength properties (JRC$_n$, JCS$_n$ γ, and Φ_b) of the study area (Valdiya 1980). These rock strength parameters are very important to maintain the stability of the steep slopes and are strongly dependent upon the lithology (Duncan 1969; Coulson 1972; Barton 1973; Barton and Choubey 1977; Bandis et al. 1983; Priest 1993; Yong et al. 2018). The maps of the JRC$_n$, JCS$_n$, γ, and Φ_b are shown in Fig. 5. The geotechnical parameters shown in Fig. 5 represent a close resemblance with the lithology of the region and their values vary with the rock mass in the study area.

The data layers (JRC$_n$, JCS$_n$, γ, Φ_b, and α) are combined by using Eq. (1) to produce the static factor of safety (F$_s$) map of the area as shown in Fig. 6. This figure shows that the (F$_s$) values range from 1 to 8.1 for the study region. The F$_s$ values around 1 indicate the instability of slopes, which is represented by the red color in the figure. In the initial step of the calculation, many grid cells of the steep slopes give the static factor of safety (F$_s$) less than 1. This indicates the instability of the slopes, but this does not necessarily mean that any ground motion can trigger these slopes and in this situation, the slopes having F$_s$ < 1, are assigned a minimal value for the static factor of safety of 1.01 (Jibson et al. 2000). This minimal value is barely above the limit equilibrium, to avoid the negative values of the critical acceleration (Jibson et al. 2000). Most of the coseismic landslides occur in the regions, where the angle of slope is at least 5°. The slope has an angle smaller than 5° and has high values of the static factor of safety, which indicates high slope stability and these slopes are unlikely to fail under the ground shaking of earthquakes (Keefer 1984). Therefore, the slopes having an angle of less than 5° are not considered in this study.

Critical acceleration

The critical acceleration map of the area was prepared by combining the static factor of the safety map and the slope angle map of the area. The critical acceleration (α_c) of the slopes is derived from the intrinsic slope properties (Topography and lithology). Therefore, the map of the critical acceleration is also known as the coseismic landslide susceptibility or dynamic slope stability (Jibson et al. 2000). The α_c values near zero in the area indicate that the more susceptible to coseismic landslides and greater than 1 g in the area shows less susceptibility for coseismic landslides (Jibson et al. 2000). The calculated values of critical acceleration (α_c) for the natural slopes of the study area are ranging from 0.005 g to 8.4 g as shown in Fig. 7.

Peak ground acceleration (PGA)

The peak ground acceleration (PGA) is an important parameter used for the landslide hazard assessment, especially in the case of earthquake-induced landslides. The PGA contour map of future scenario earthquakes of magnitude 7.0, 8.0, and 8.6 (M_w) is employed for the present study region. An earthquake (M_w 5.4) that occurred on 04 April 2011 is simulated for the Kumaun region by Sandeep et al. (2019), which has an epicentral location (29.698° N and 80.754° E) adjacent to the present study region. The same location is considered for the simulation of future earthquakes (7.0, 8.0, and 8.6 M_w) (Sandeep et al. 2019). To prepare the PGA contour map, the whole study region is divided into 0.1 × 0.1° grid and the PGA value is simulated at each grid point (Sandeep et al. 2019). The

Fig. 4 The slope angle map derived from the high-resolution DEM of the study area

Slope angle
- < 10°
- 11° - 20°
- 21° - 30°
- 31° - 40°
- 41° - 50°
- 51° - 60°
- 61° - 70°
- > 70°
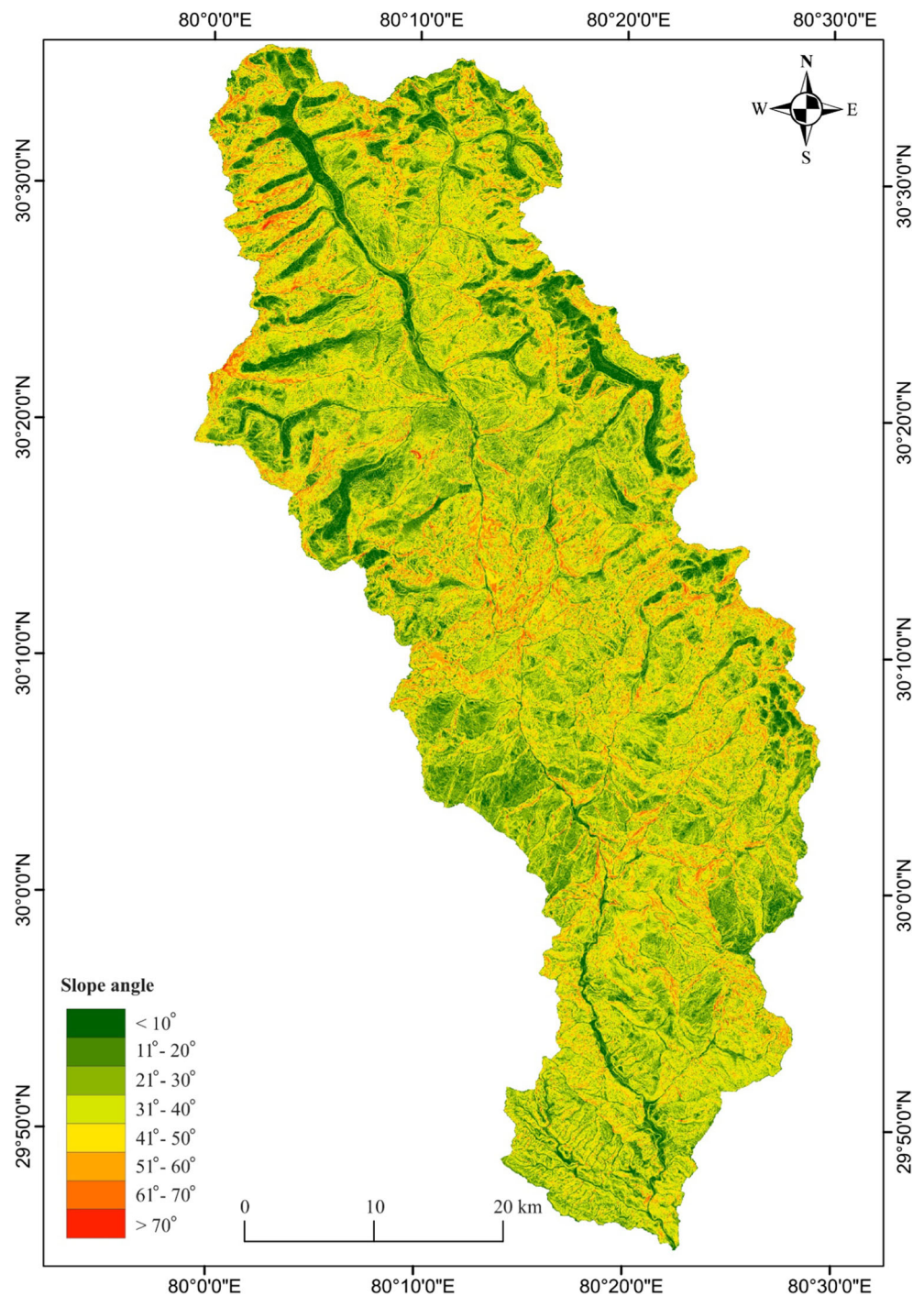
estimated PGA values at each grid point are further used to prepare the acceleration map for future earthquakes of magnitude 7.0, 8.0, and 8.6 (Fig. 8). Figure 8 shows the distribution of PGA values in the study region, which indicates that these values are increasing with the increase of magnitude of the earthquake. It also represents the decrement of PGA values from SE to NW direction of the study region as we move away from the epicenter of the earthquake.

Newmark's permanent displacement

The Newmark's permanent displacement is the predicted slope failure distribution due to the ground shaking. The Newmark permanent displacement of each grid cell in the area has been calculated by combining layers of critical acceleration, peak ground acceleration, and moment magnitude of an earthquake by using Eq. (3). The predicted permanent
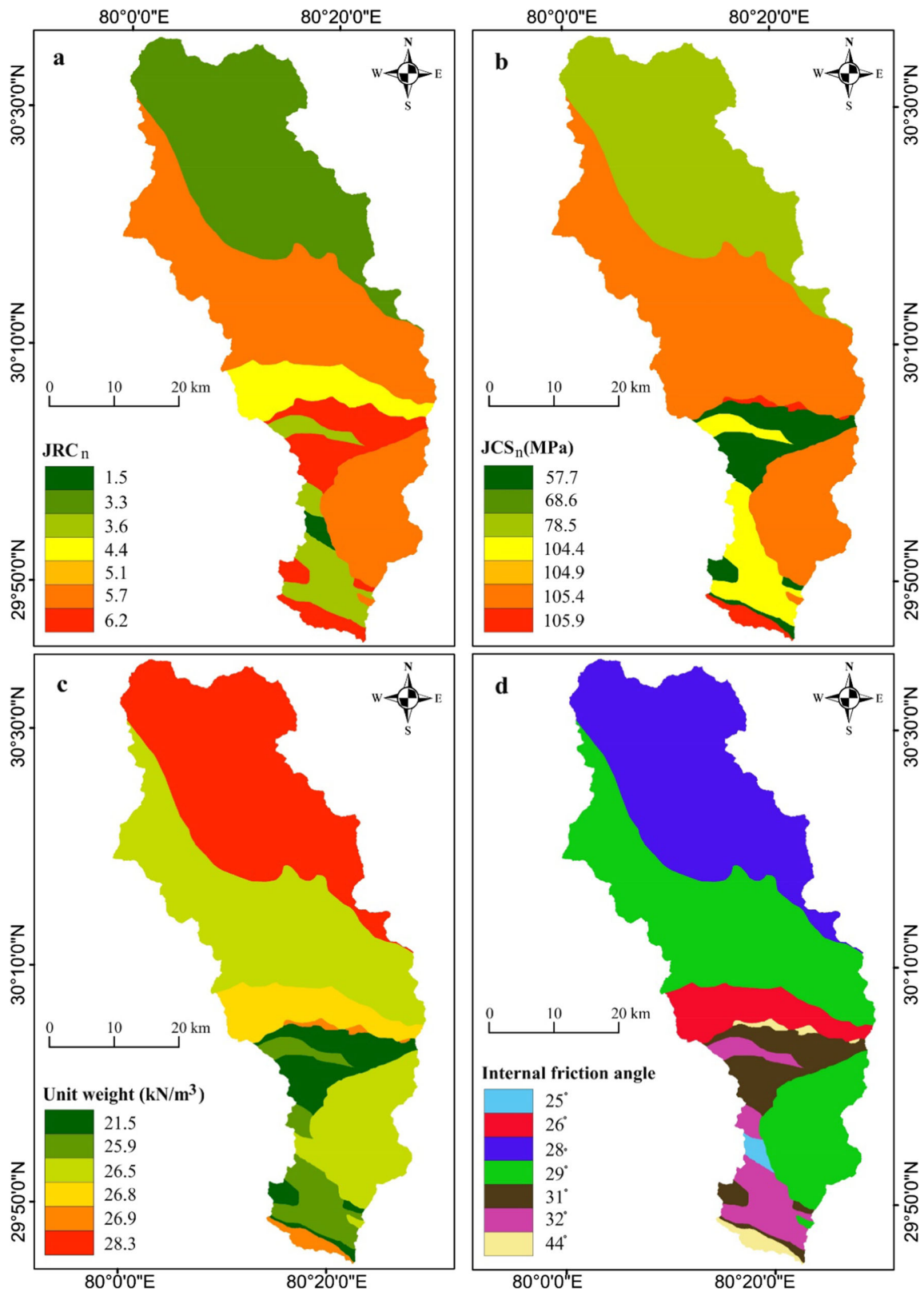
Fig. 5 The map of geotechnical parameters of rock mass of study region (**a**) joint roughness coefficient (JRC$_n$), (**b**) joint surface compressive (JCS$_n$), (**c**) Unit weight (γ), and (**d**) friction angle (Φ_b)
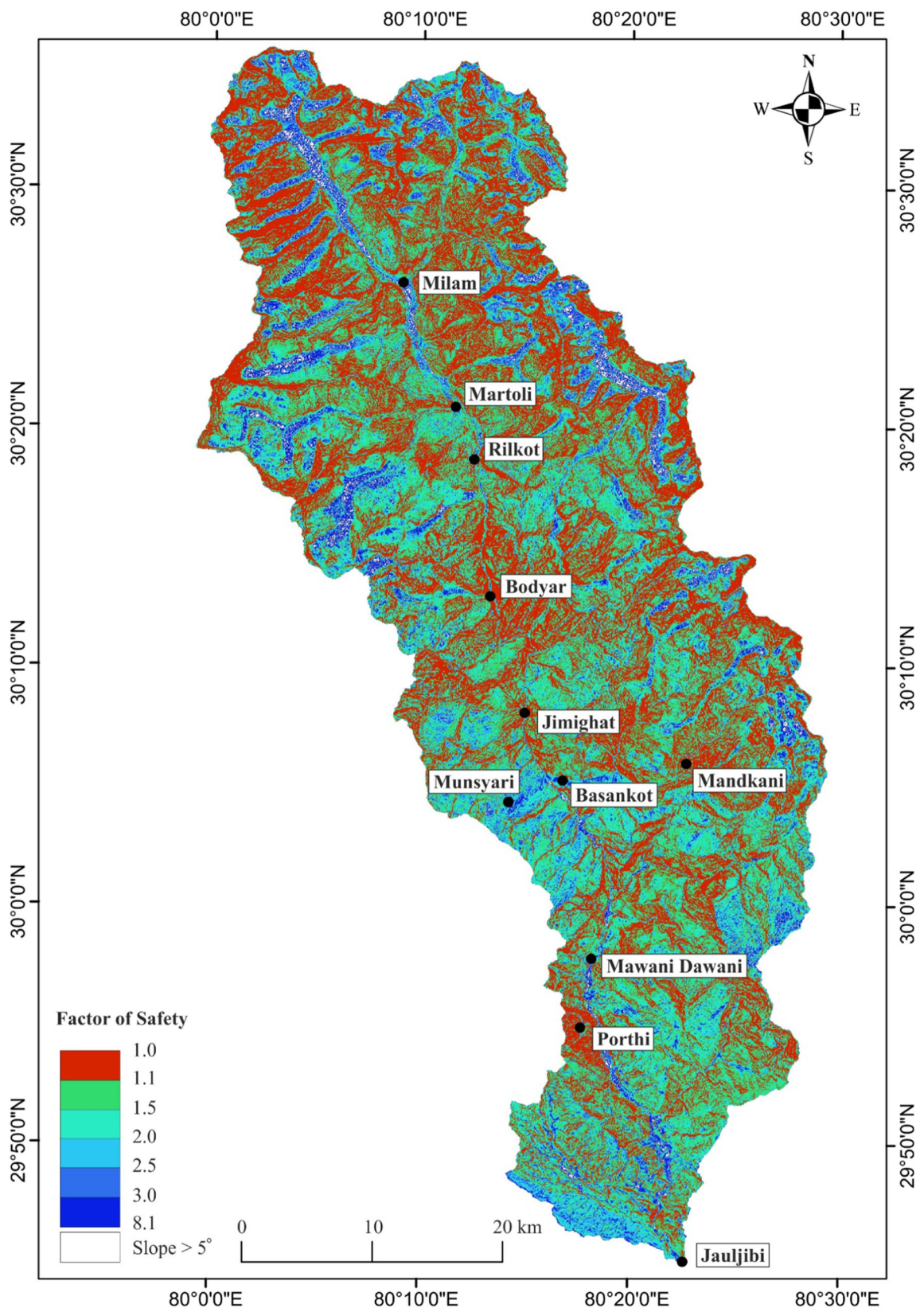
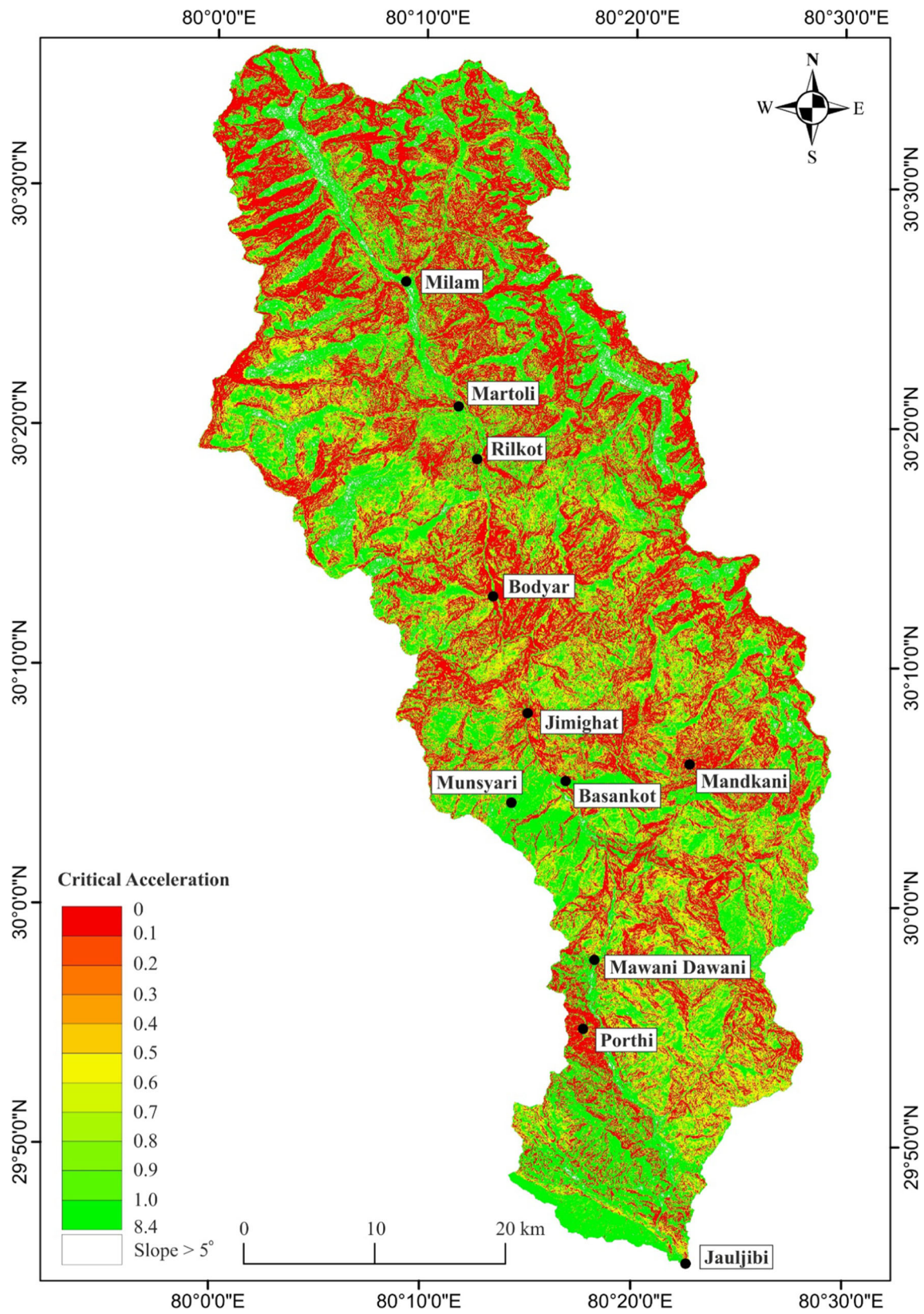**Fig. 6** The map of the static factor of safety of the slopes for the study area

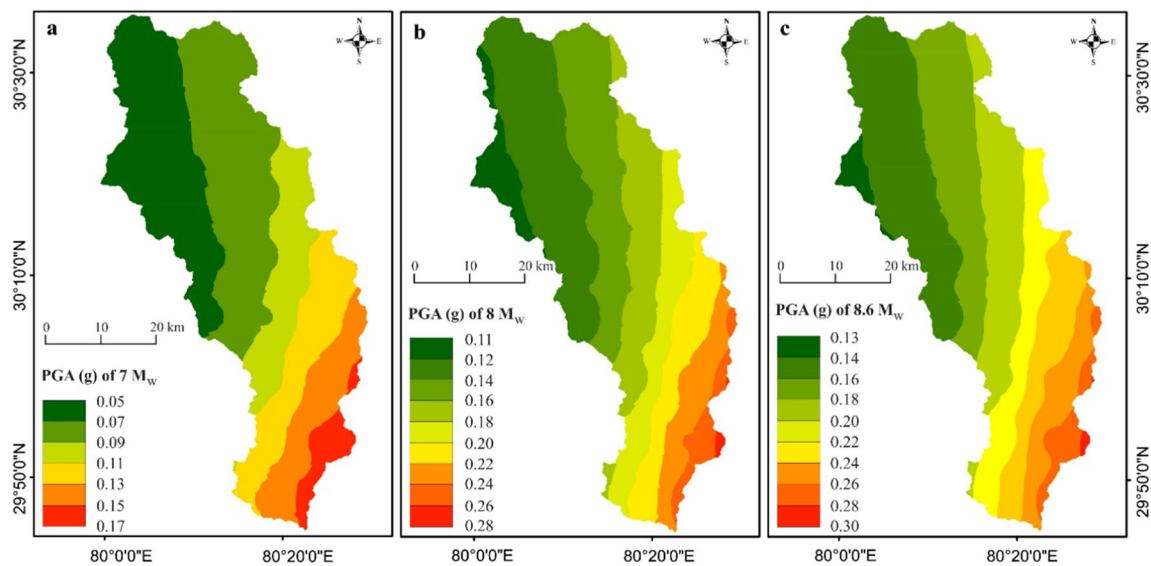**Fig. 7** The map of the critical acceleration of slopes present in the study area

Fig. 8 The map of the peak ground acceleration (PGA), produced by the simulated earthquakes of magnitude (M_w) (**a**) 7.0, (**b**) 8.0, and (**c**) 8.6, respectively

displacement map for the simulated earthquakes of magnitude 7.0, 8.0, and 8.6 (M_w) are shown in Figs. 9, 10, and 11.

Discussion

It has been observed that the static factor of safety of the slopes is varying with the rock materials and the angle of slopes in the study area. Similar observation has also been documented by many researchers for different parts of the globe like the San Francisco East Bay Hill region, California (Miles and Ho 1999), the Northridge region, California (Jibson et al. 2000), Chi-Chi region, Taiwan (Wang and Lin 2010), Mid Niigata region, Japan (Shinoda and Miyata 2017), Hong Kong region (Huang et al. 2020), and Ludian region, China (Zang et al. 2020). The slopes with the static factor of safety (F_s) with a value 1 or very close to 1 are highly probable to fail and the values greater than 1 are less susceptible to failures (Jibson et al. 2000). In the present study, Porthi village in the southern part, Basankot village, Jimighat village and Mandkani village in the central part, Bodyar village, Martoli village, Rilkot, and surroundings of Milam village in the northern parts show the low values of F_s (Fig. 6). This is because of the presence of low-strength rock materials such as slate, sheared schistose gneiss, and phyllite in these regions (Valdiya 1980; Valdiya 2001; Luirei et al. 2006). These areas also consist of steeper slopes with highly jointed and fractured rock materials as compared to other parts of the study region. Further, in the northern region, the surroundings of Milam village, Rilkot village, Martoli village, and Bodyar village, in the central region near Munsiyari Thrust (Basankot and Madkani village) and Vaikrita Thrust (Jimighat village), and the area of Porthi village in the lower parts of the study region show low values

for the critical acceleration (a_c) that means these regions are dynamically susceptible to failures. This is mainly because of the presence of weak rock types and steep slope topography in areas (Valdiya 1980; Jibson et al. 2000; Valdiya 2001; Luirei et al. 2006). The distribution of the seismic landslide susceptibility or dynamic slope stability of the study area is shown in Fig. 7. In the present work, the PGA value distribution is also computed and lies in the range of 0.05 to 0.30 g for the study region. The present study region has the probability of an earthquake of intensity IX and the PGA value for the Himalayan region with seismic intensity IX is 0.16 g. (Panjamani et al., 2016). Hence, the obtained PGA values justify that the present region lies in the zone of seismic intensity IX.

Newmark's permanent displacement maps are prepared by using Eq. (3) for future scenario earthquakes (M_w = 7.0, 8.0, and 8.6) and shown in Figs. 9, 10, and 11, respectively. These maps have displacement up to 76, 279, and 502 cm for the simulated earthquakes 7.0, 8.0, and 8.6 (M_w), respectively. To check the effect of the worst condition, scenario earthquake of 8.6 magnitude is considered, which is equivalent to the Assam 1950 earthquake, the highest magnitude earthquake that occurred in the Himalayan belt (Srivastava et al., 2013; Gupta and Gahalaut, 2015). Zang et al. (2020) have been observed that the majority of landslides fall under Newmark's permanent displacement greater than 40 cm and few landslides fall under <40 cm displacement value during the Ludian earthquake of 2011 (6.1 M_w). In the present work, the region having the Newmark's permanent displacement value greater than 40 cm is classified as a high slope displacement region. Newmark's permanent displacement map obtained by using the earthquake of magnitude 7 indicates that the 14% area showing high values of
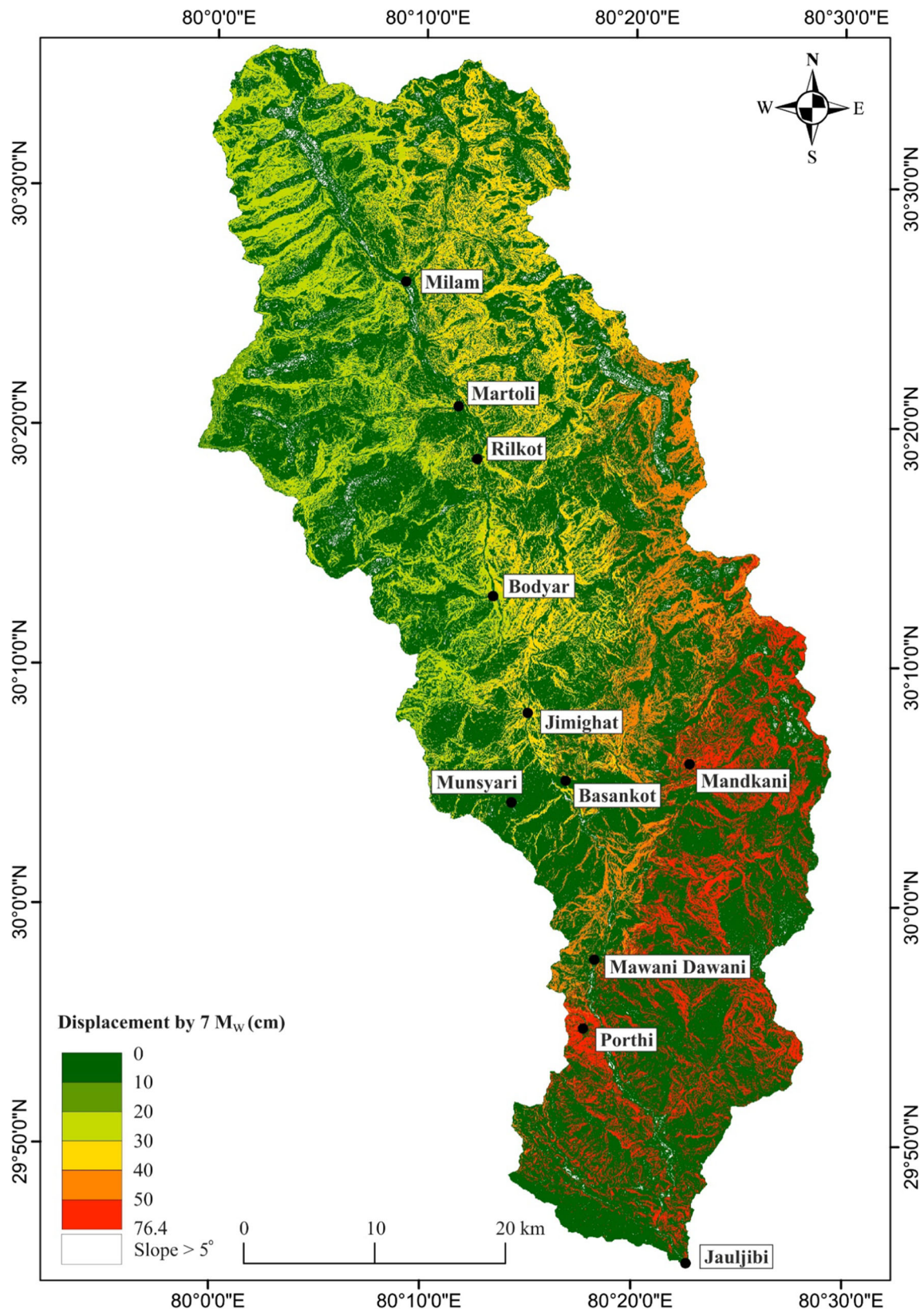
Fig. 9 The map of the predicted Newmark's permanent displacements during the earthquake magnitude of 7.0 (M$_w$)

slope displacement (>40 cm) in the South and southeast parts as compared to the Northern and northwest parts of the study area. The predicted Newmark's permanent displacement maps depict that the 36 and 41% area (>40 cm)
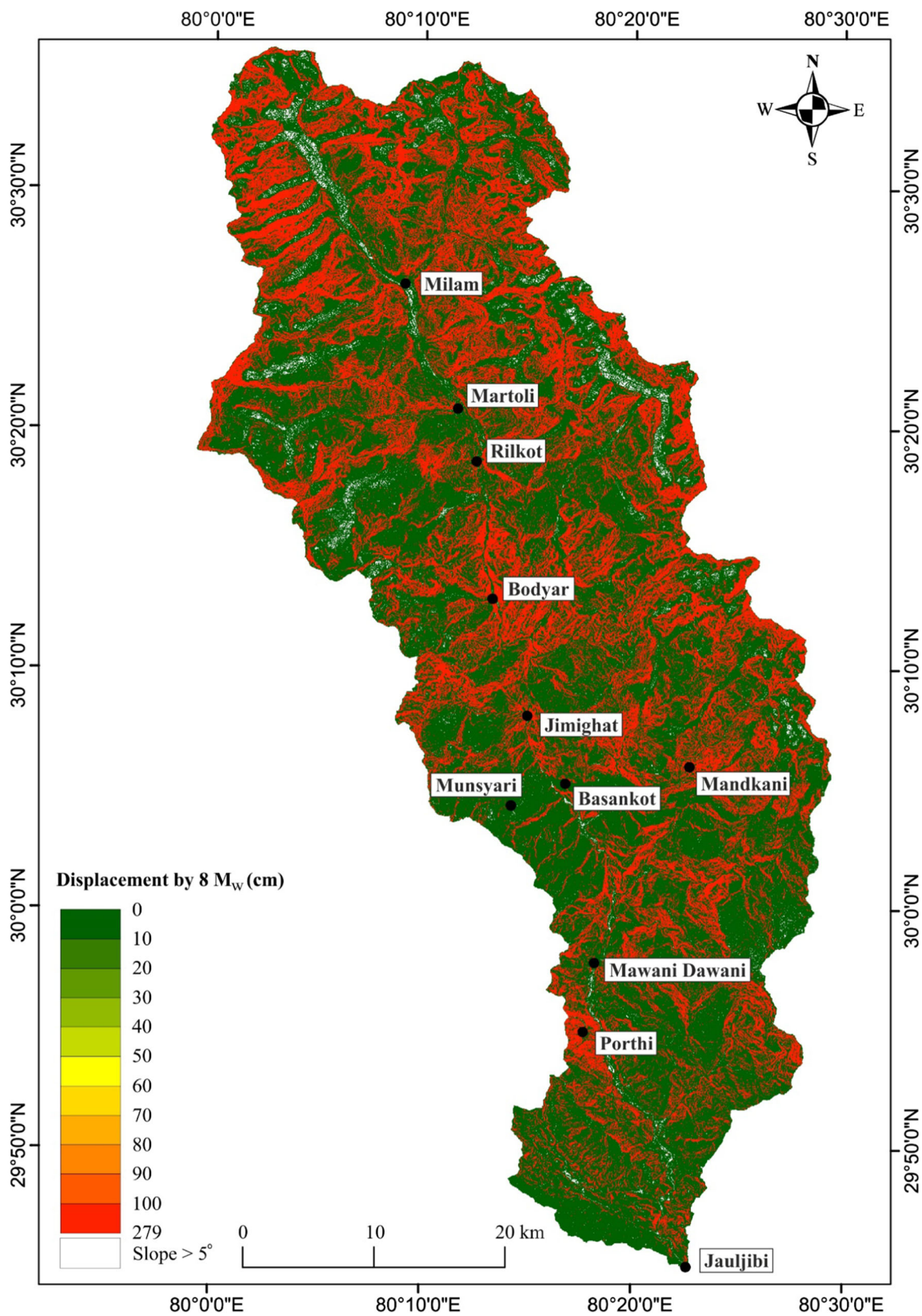
Fig. 10 The map of the predicted Newmark's permanent displacements during the earthquake magnitude of 8.0 (M_w)

falls under the high slope displacement classes for magnitude 8.0 and 8.6, respectively. In the Newmark displacement maps, the existence of the region with low values of slope displacement value may be due to the presence of gentle to moderate
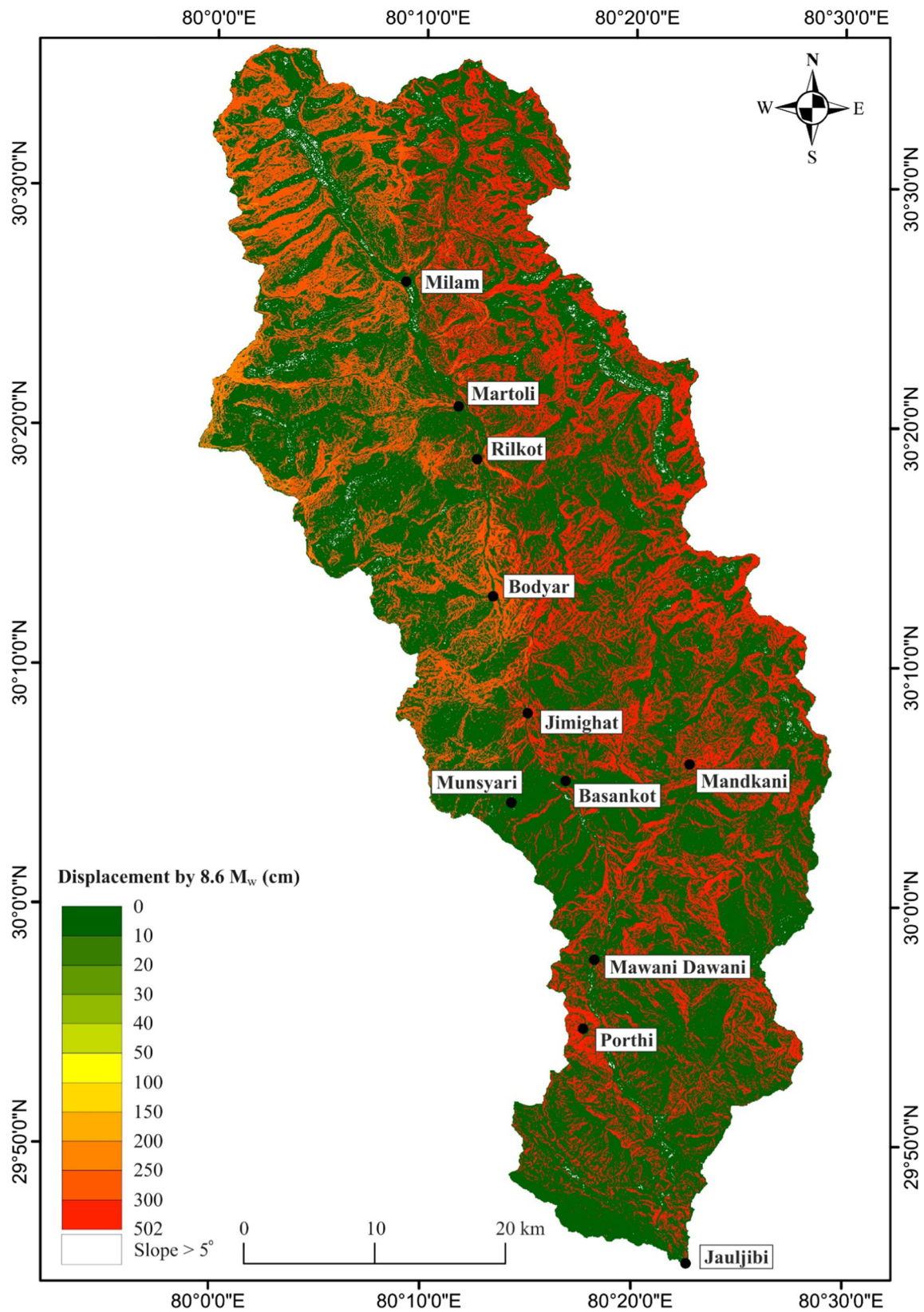
Fig. 11 The map of the predicted Newmark's permanent displacements during the earthquake magnitude of 8.6 (M_w)

slopes and strong rock material. As gentle slopes and steep slopes with strong rock material are not susceptible to slope failures due to the earthquake ground shaking (Keefer 1984; Jibson et al. 2000; Zang et al. 2020).

A number of studies regarding earthquake-induced landslides have been carried out worldwide (Jibson et al. 2000; Ingles et al. 2006; Wang and Lin 2010; Papathanassiou 2012; Shinoda and Miyata 2017; Liu et al. 2018; Wang et al. 2019; Zang et al. 2020; Yang et al. 2021). All the aforementioned studies are based on the post-earthquake occurrence that means landslide studies have been carried out after the occurrence of an earthquake. Whereas, the present study is based on the occurrence of landslides due to future scenario earthquakes. In the present work, the simulated earthquake epicenters are located on the southeast side of the study area (Fig. 1). So, the maximum ground shaking occurred near the epicenter and decreases as going away from it (Wilson and Keefer 1983). As shown in Figs. 9, 10, and 11, the largest predicted displacements or earthquake-induced landslides have been observed for the simulated earthquake of magnitude 8.6 M_w followed by earthquakes of 7.0 and 8.0 (M_w) magnitude, and this difference is because of large magnitude.

Conclusions

The present study exhibits preparation of coseismic landslide susceptibility or dynamic slope stability mapping and the spatial probability of slope displacements due to the ground shaking of earthquake magnitudes 7.0, 8.0, and 8.6 (M_w) by using Newmark's analysis. The study draws the following conclusions:

- This work is the first of its kind in the Himalaya region, in which earthquake-induced landslides have been explored in view of future major to great probabilistic earthquakes.
- The shear strength parameters, such as the joint roughness coefficient (JRC) and joint surface compressive strength (JCS) are considered to provide more reliable results in the form of the dynamic slope stability map.
- The high coseismic landslide susceptible zone (Newmark's permanent displacement value greater than 40 cm) covers the area about 300 km^2, 785 km^2, and 894 km^2 for the earthquakes magnitude 7.0, 8.0, and 8.6 (M_w), respectively.
- The earthquake's magnitudes 7.0, 8.0, and 8.6 (M_w) might moderately (Newmark's permanent displacement value <40 cm) damage the area about 1459 km^2, 1256 km^2, and 1134 km^2 in the study region, respectively.

References

Bandis SC, Lumsdent AC, Barton NR (1983) Fundamentals of rock joint deformation. Int J Rock Mech Min Sci Geomech Abstr 20:249–268. https://doi.org/10.1016/0148-9062(83)90595-8

Barton N (1971) A relationship between joint roughness and joint shear strength. Rock Fract Int Symp Rock Mech Nancy Fr paper1-8

Barton N (1973) Review of a new shear-strength criterion for rock joints. Eng Geol 7:287–332

Barton N, Choubey V (1977) The shear strength of rock joints in theory and practice. Rock Mech Felsmechanik Mécanique des Roches 10:1–54. https://doi.org/10.1007/BF01261801

BIS Code 1893 (2002) Earthquake hazard zoning map of India. www.bis.org.in

Chen X, Liu C, Wang M (2019) A method for quick assessment of earthquake-triggered landslide hazards: a case study of the Mw6.1 2014 Ludian, China earthquake. Bull Eng Geol Environ 78:2449–2458. https://doi.org/10.1007/s10064-018-1313-7

Chen X, Chen J, Cui P et al (2018) Assessment of prospective hazards resulting from the 2017 earthquake at the world heritage site Jiuzhaigou Valley, Sichuan, China. J Mt Sci 15:779–792. https://doi.org/10.1007/s11629-017-4785-1

Coulson JH (1972) Shear strength of flat surfaces in rock. Proc 13th Symp On Rock Mech Urbana, Ill:77–105

Cruden DM (1991) A simple definition of a landslide. Bull Int Assoc Eng Geol - Bull l'Association Int Géologie l'Ingénieur 43:27–29. https://doi.org/10.1007/BF02590167

Duncan N, Sheerman-Chase A (1965-1966) Planning design and construction-rock mechanics in civil engineering works. Civ Eng Public Work Rev 61:213–215

Duncan N (1969) Engineering geology and rock mechanics, vol 1 and 2

Dunning SA, Mitchell WA, Rosser NJ, Petley DN (2007) The Hattian Bala rock avalanche and associated landslides triggered by the Kashmir earthquake of 8 October 2005. Eng Geol 93:130–144. https://doi.org/10.1016/j.enggeo.2007.07.003

Gallen SF, Clark MK, Godt JW et al (2017) Application and evaluation of a rapid response earthquake-triggered landslide model to the 25 April 2015 Mw 7.8 Gorkha earthquake, Nepal. Tectonophysics 714–715:173–187. https://doi.org/10.1016/j.tecto.2016.10.031

Gupta HK, Gahalaut VK (2015) Can an earthquake of Mw~ 9 occur in the Himalayan region? Geol Soc Lond, Spec Publ 412:43–53

Guzzetti F, Cardinali M, Reichenbach P (1994) The AVI project: a bibliographical and archive inventory of landslides and floods in Italy. Environ Manag 18:623–633. https://doi.org/10.1007/BF02400865

Haque U, Da Silva PF, Devoli G, Pilz J, Zhao B, Khaloua A et al (2019) The human cost of global warming: deadly landslides and their triggers (1995–2014). Sci Total Environ 682:673–684

Horn BK (1981) Hill shading and the reflectance map. Proc IEEE 69:14–47

Huang D, Wang G, Du C et al (2020) An integrated SEM-Newmark model for physics-based regional coseismic landslide assessment. Soil Dyn Earthq Eng 132:106066. https://doi.org/10.1016/j.soildyn.2020.106066

Hung C, Lin GW, Syu HS et al (2018) Analysis of the Aso-Bridge landslide during the 2016 Kumamoto earthquakes in Japan. Bull Eng Geol Environ 77:1439–1449. https://doi.org/10.1007/s10064-017-1103-7

Ingles J, Darrozes J, Soula JC (2006) Effects of the vertical component of ground shaking on earthquake-induced landslide displacements using generalized Newmark analysis. Eng Geol 86:134–147. https://doi.org/10.1016/j.enggeo.2006.02.018

Jibson RW (2011) Methods for assessing the stability of slopes during earthquakes—a retrospective. Eng Geol 122:43–50. https://doi.org/10.1016/j.enggeo.2010.09.017

Jibson RW, Harp EL, Michael JA (2000) A method for producing digital probabilistic seismic landslide hazard maps. Eng Geol 58:271–289. https://doi.org/10.1016/S0013-7952(00)00039-9

Joshi A, Kumar P, Mohanty M et al (2012) Determination of Q β(f) in different parts of Kumaon Himalaya from the inversion of spectral acceleration data. Pure Appl Geophys 169:1821–1845. https://doi.org/10.1007/s00024-011-0421-0

Keefer DK (1984) Landslides caused by earthquakes. Geol Soc Am Bull 95(4):406–421

Khattri KM, Tyagi AK (1983) Seismicity patterns in the Himalayan plate boundary and identification of the areas of high seismic potential. Tectonophysics 96:281–297. https://doi.org/10.1016/0040-1951(83)90222-6

Kumar P, Joshi A, Sandeep et al (2015) Detailed attenuation study of shear waves in the Kumaon Himalaya, India, using the inversion of strong-motion data. Bull Seismol Soc Am 105:1836–1851. https://doi.org/10.1785/0120140053

Lin ML, Tung CC (2004) A GIS-based potential analysis of the landslides induced by the Chi-Chi earthquake. Eng Geol 71:63–77. https://doi.org/10.1016/S0013-7952(03)00126-1

Liu J, Shi J, Wang T, Wu S (2018) Seismic landslide hazard assessment in the Tianshui area, China, based on scenario earthquakes. Bull Eng Geol Environ 77:1263–1272. https://doi.org/10.1007/s10064-016-0998-8

Luirei K, Pant PD, Kothyari GC (2006) Geomorphic evidences of neotectonic movements in Dharchula area, northeast Kumaun: a perspective of the recent tectonic activity. J Geol Soc India 67:92–100

Ma S, Xu C (2019) Assessment of co-seismic landslide hazard using the Newmark model and statistical analyses: a case study of the 2013 Lushan, China, Mw6.6 earthquake. Nat Hazards 96:389–412. https://doi.org/10.1007/s11069-018-3548-9

Martha TR, Babu Govindharaj K, Vinod Kumar K (2015) Damage and geological assessment of the 18 September 2011 Mw 6.9 earthquake in Sikkim, India using very high resolution satellite data. Geosci Front 6:793–805. https://doi.org/10.1016/j.gsf.2013.12.011

Miles SB, Ho CL (1999) Rigorous landslide hazard zonation using Newmark's method and stochastic ground motion simulation. Soil Dyn Earthq Eng 18:305–323. https://doi.org/10.1016/S0267-7261(98)00048-7

Monika, Kumar P, Sandeep et al (2020) Spatial variability studies of attenuation characteristics of Qα and Qβ in Kumaon and Garhwal region of NW Himalaya. Nat Hazards 103:1219–1237. https://doi.org/10.1007/s11069-020-04031-7

Neuland H (1976) A prediction model of landslips. Catena 3:215–230. https://doi.org/10.1016/0341-8162(76)90011-4

Newmark NM (1965) Effects of earthquakes on dams and embankments. Geotechnique 15:139–160. https://doi.org/10.1680/geot.1965.15.2.139

Nilsen TH, Brabb EE (1977) Slope-stability studies in the San Francisco Bay region, California. GSA Rev Eng Geol 3:233–243. https://doi.org/10.1130/REG3-p233

Okimura T, Kawatani T (1987) Mapping of the potential surface-failure sites on granite slopes. In: Gardiner E (ed) International Geomorphology 1986, PartI, Wiley, Chichester, pp 121–1381

Owen LA, Kamp U, Khattak GA et al (2008) Landslides triggered by the 8 October 2005 Kashmir earthquake. Geomorphology 94:1–9. https://doi.org/10.1016/j.geomorph.2007.04.007

Panjamani A, Bajaj K, Moustafa SSR, Al-Arifi NSN (2016) Relationship between intensity and recorded ground-motion and spectral parameters for the Himalayan Region. Bull Seismol Soc Am 106:1672–1689

Papathanassiou G (2012) Estimating slope failure potential in an earthquake prone area: a case study at Skolis Mountain, NW Peloponnesus, Greece. Bull Eng Geol Environ 71:187–194. https://doi.org/10.1007/s10064-010-0344-5

Priest SD (1993) Discontinuity analysis for rock engineering. Pergamon

Qi SW, Yan C, Liu C (2012) Two typical types of earthquake triggered landslides and their mechanisms. In: Landslides and Engineered Slopes: Protecting Society through Improved Understanding - Proceedings of the 11th International and 2nd North American Symposium on Landslides and Engineered Slopes, 2012. pp 1819–1823

Raj KBG (2011) Recession and reconstruction of Milam Glacier, Kumaon Himalaya, observed with satellite imagery. Curr Sci: 1420–1425

Rathje EM, Saygili G (2009) Probabilistic assessment of earthquake-induced sliding displacements of natural slopes. Bull N Z Soc Earthq Eng 42:18–27. https://doi.org/10.5459/bnzsee.42.1.18-27

Roback K, Clark MK, West AJ et al (2018) The size, distribution, and mobility of landslides caused by the 2015 Mw7.8 Gorkha earthquake, Nepal. Geomorphology 301:121–138. https://doi.org/10.1016/j.geomorph.2017.01.030

Romeo R (2000) Seismically induced landslide displacements: a predictive model. Eng Geol 58:337–351. https://doi.org/10.1016/S0013-7952(00)00042-9

Sandeep JA, Sah SK et al (2019) Modeling of 2011 IndoNepal earthquake and scenario earthquakes in the Kumaon Region and comparative attenuation study using PGA distribution with the Garhwal Region. Pure Appl Geophys 176:4687–4700. https://doi.org/10.1007/s00024-019-02232-1

Shinoda M, Miyata Y (2017) Regional landslide susceptibility following the Mid NIIGATA prefecture earthquake in 2004 with NEWMARK'S sliding block analysis. Landslides 14:1887–1899. https://doi.org/10.1007/s10346-017-0833-8

Srivastava HN, Bansal BK, Verma M (2013) Largest earthquake in Himalaya: an appraisal. J Geol Soc India 82:15–22

Valdiya KS (2001) Reactivation of terrane-defining boundary thrusts in central sector of the Himalaya: implications. Curr Sci 81:1418–1431

Valdiya KS (1980) Geology of kumaun lesser Himalaya. Wadia Inst Himal Geol Rajpur Road Dehradun Himachal times Press 280

Van Westen CJ, Soeters R, Sijmons K (2000) Digital geomorphological landslide hazard mapping of the Alpago area, Italy. ITC J 2:51–60. https://doi.org/10.1016/S0303-2434(00)85026-6

Wald DJ, Quintoriano V, Heaton TH, Kanamori H (1999) Relationships between peak ground acceleration, peak ground velocity, and Modified Mercalli intensity in California. Earthquake Spectra 15:557–564

Wang F, Fan X, Yunus AP et al (2019) Coseismic landslides triggered by the 2018 Hokkaido, Japan (Mw 6.6), earthquake: spatial distribution, controlling factors, and possible failure mechanism. Landslides 16:1551–1566. https://doi.org/10.1007/s10346-019-01187-7

Wang KL, Lin ML (2010) Development of shallow seismic landslide potential map based on Newmark's displacement: the case study of Chi-Chi earthquake, Taiwan. Environ Earth Sci 60:775–785. https://doi.org/10.1007/s12665-009-0215-1

Wilson RC, Keefer DK (1983) Dynamic analysis of a slope failure from the 6 August 1979 Coyote Lake, California, earthquake. Seismological Society of America 73(3):863–877

Wu JH, Chen CH (1979) Force-based and displacement-based back analysis of shear strengths: case of Tsaoling landslide. WSEAS Trans Adv Eng Educ 5:200–209

Wu JH, Lin HM (2008) Analyzing the shear strength parameters of the Chiu-fen-erh-shan landslide: integrating strong-motion and GPS data to determine the best-fit accelerogram. GPS Solutions 13(2):153–163

Wu JH, Chen CH (2009) Back calculating the seismic shear strengths of the Tsaoling landslide associated with accelerograph and GPS data. Iran J Sci Technol Transac B Eng 33(B4):301

Wu JH, Tsai PH (2011) New dynamic procedure for back-calculating the shear strength parameters of large landslides. Eng Geol 123:129–147

Xu C, Xu X, Yu G (2013) Landslides triggered by slipping-fault-generated earthquake on a plateau: an example of the 14 April 2010, Ms 7.1, Yushu, China earthquake. Landslides 10:421–431. https://doi.org/10.1007/s10346-012-0340-x

Yadav RR, Misra KG, Kotlia BS, Upreti N (2014) Premonsoon precipitation variability in Kumaon Himalaya, India over a perspective of ~300 years. Quat Int 325:213–219

Yang Q, Zhu B, Hiraishi T (2021) Probabilistic evaluation of the seismic stability of infinite submarine slopes integrating the enhanced Newmark method and random field. Bull Eng Geol Environ:1–19. https://doi.org/10.1007/s10064-020-02058-5

Yiğit A (2020) Prediction of amount of earthquake-induced slope displacement by using Newmark method. Eng Geol 264:105385. https://doi.org/10.1016/j.enggeo.2019.105385

Yin KL, Yan TZ (1988) Statistical prediction models for slope instability of metamorphosed rocks. Landslides Proc 5th Symp Lausanne 2: 1269–1272. https://doi.org/10.1016/0148-9062(90)90358-9

Yin Y, Wang F, Sun P (2009) Landslide hazards triggered by the 2008 Wenchuan earthquake, Sichuan, China. Landslides 6:139–152. https://doi.org/10.1007/s10346-009-0148-5

Yong R, Ye J, Liang QF et al (2018) Estimation of the joint roughness coefficient (JRC) of rock joints by vector similarity measures. Bull Eng Geol Environ 77:735–749. https://doi.org/10.1007/s10064-016-0947-6

Youd TL (1985) Landslides caused by earthquakes: discussion. Bull Geol Soc Am 96:1091–1092

Zang M, Qi S, Zou Y et al (2020) An improved method of Newmark analysis for mapping hazards of coseismic landslides. Nat Hazards Earth Syst Sci 20:713–726. https://doi.org/10.5194/nhess-20-713-2020

Zhou S, Chen G, Fang L (2016) Distribution pattern of landslides triggered by the 2014 Ludian earthquake of China: implications for regional threshold topography and the Seismogenic fault identification. ISPRS Int J Geo-Inform 5:46. https://doi.org/10.3390/ijgi5040046